Neurobiology of Disease

Diffusion Tensor Tractography Reveals Abnormal Topological Organization in Structural Cortical Networks in Alzheimer's Disease

Chun-Yi Lo,[1] **Pei-Ning Wang,**[2,3] **Kun-Hsien Chou,**[4] **Jinhui Wang,**[5] **Yong He,**[5] and **Ching-Po Lin**[1,6]

[1]Department of Biomedical Imaging and Radiological Sciences, National Yang-Ming University, Taipei 11221, Taiwan, [2]Department of Neurology, National Yang-Ming University School of Medicine, Taipei 11221, Taiwan, [3]Department of Neurology, Taipei Veterans General Hospital, Taipei 11221, Taiwan, [4]Institute of Biomedical Engineering, National Yang-Ming University, Taipei 11221, Taiwan, [5]State Key Laboratory of Cognitive Neuroscience and Learning, Beijing Normal University, Beijing, China 100875, and [6]Brain Connectivity Laboratory, Institute of Neuroscience, National Yang-Ming University, Taipei 11221, Taiwan

Recent research on Alzheimer's disease (AD) has shown that the decline of cognitive and memory functions is accompanied by a disrupted neuronal connectivity characterized by white matter (WM) degeneration. However, changes in the topological organization of WM structural network in AD remain largely unknown. Here, we used diffusion tensor image tractography to construct the human brain WM networks of 25 AD patients and 30 age- and sex-matched healthy controls, followed by a graph theoretical analysis. We found that both AD patients and controls had a small-world topology in WM network, suggesting an optimal balance between structurally segregated and integrative organization. More important, the AD patients exhibited increased shortest path length and decreased global efficiency in WM network compared with controls, implying abnormal topological organization. Furthermore, we showed that the WM network contained highly connected hub regions that were predominately located in the precuneus, cingulate cortex, and dorsolateral prefrontal cortex, which was consistent with the previous diffusion-MRI studies. Specifically, AD patients were found to have reduced nodal efficiency predominantly located in the frontal regions. Finally, we showed that the alterations of various network properties were significantly correlated with the behavior performances. Together, the present study demonstrated for the first time that the Alzheimer's brain was associated with disrupted topological organization in the large-scale WM structural networks, thus providing the structural evidence for abnormalities of systematic integrity in this disease. This work could also have implications for understanding how the abnormalities of structural connectivity in AD underlie behavioral deficits in the patients.

Introduction

Alzheimer's disease (AD) is an irreversible neurodegenerative disease characterized by progressive deterioration of cognitive and memory functions. There is a growing body of evidence suggesting that the cognitive decline may arise from integrative abnormalities between functionally and/or anatomically related brain regions. The biological hypothesis of AD as a disconnection syndrome involves progressive biochemical and structural changes, which begin at the cellular and synaptic level, and ultimately culminate in neuronal death and white matter (WM) de-

generation (Brun and Englund, 1986; Selkoe, 2002; Delbeuck et al., 2003; Pievani et al., 2010).

Diffusion tensor imaging (DTI) is a noninvasive technique that can be used to reflect the microstructural tissue status and orientations. The orientations of WM pathways can also be inferred by the principal eigenvector of the diffusion tensor (Basser et al., 1994), which provides a new opportunity to investigate WM pathways in living humans (for review, see Mori and van Zijl, 2002). In AD patients, neural degenerations have been identified in a variety of WM tracts, including the corpus callosum (Rose et al., 2000; Naggara et al., 2006; Ukmar et al., 2008) and posterior cingulate fasciculus (Kiuchi et al., 2009). Despite these advances for alterations of specific tracts, however, little is known about the abnormalities of topological organization in WM network in AD.

Recent studies have suggested that structural networks of the human brain can be constructed from diffusion MRI tractography and further characterized by using graph theoretical approaches [for review, see Bullmore and Sporns (2009) and He and Evans (2010)]. Through these approaches, WM network of human brain has been found to have a "small-world" topology (Hagmann et al., 2007, 2008; Iturria-Medina et al., 2008; Gong et al., 2009b), characterized by a high degree of local interconnec-

Table 1. Demographic and clinical characteristics of participants

Characteristic	Patients	Controls	*p* value
Age	79.40 (5.89)	77.07 (6.37)	0.169
Female/male	10/15	11/19	0.800
MMSE	20.92 (2.36)	28.83 (0.99)	$<1.0 \times 10^{-22}$
CVLT-TC	16.40 (3.62)	29.77 (3.60)	$<1.0 \times 10^{-18}$
CVLT-SD	3.40 (1.71)	8.40 (0.77)	$<1.0 \times 10^{-19}$
CVLT-LD	1.08 (1.53)	8.30 (0.75)	$<1.0 \times 10^{-28}$
CFT-delay	0.68 (1.28)	10.90 (3.79)	$<1.0 \times 10^{-17}$

Scores are shown with mean (SD).

tivity and small path lengths linking individual network nodes (Watts and Strogatz, 1998). It is worthy to note that these diffusion-MRI studies have consistently demonstrated that the human WM network contains highly connected hub regions predominately located in the precuneus (PCUN), posterior cingulate gyrus (PCG), and medial prefrontal cortex (Hagmann et al., 2008; Gong et al., 2009b; Yan et al., 2010). Relating to AD, several studies have demonstrated small-world alterations in functional (Stam et al., 2007, 2009; Supekar et al., 2008; de Haan et al., 2009) and morphological (He et al., 2008) brain networks, but the results were substantially inconsistent (we will return to this issue in the Discussion section). To our knowledge, no studies reported AD-related changes in the topological properties in WM network.

Here, we used DTI tractography and graph theoretical approaches to investigate changes in topological organization of WM network in AD patients. As described above, AD is a neurodegenerative disease associated with the WM abnormalities that might interrupt neuronal connections. In this study, we therefore sought to determine whether AD patients would show (1) abnormal small-world organization and reduced network efficiency in WM network; (2) altered nodal efficiency in WM network; and (3) significant correlations between network property changes and behavioral/clinical variables.

Materials and Methods

Participants

The study includes 25 AD patients (female/male: 10/15; mean age: 79.4; SD: 5.89) and 30 age- and sex-matched normal controls (NCs) (female/male: 11/19; mean age 77.07; SD 6.37), which were recruited from the Taipei Veterans General Hospital in Taiwan. All subjects and the guardians of AD patients had given written informed consent before participating in the study. The diagnosis for AD is based on the criteria of National Institute of Neurological and Communicative Disorders and Stroke/Alzheimer's Disease and Related Disorders Association (McKhann et al., 1984) for probable AD. All AD patients underwent neurological examinations, laboratory tests, and neuroimaging evaluation to exclude patients with secondary causes of dementia, such as vascular dementia, Parkinson's disease, hypothyroidism, vitamin B_{12} deficiency, and syphilis. The severity of dementia was evaluated with Clinical Dementia Rating (CDR) scale (Morris, 1993), and all AD patients were mild AD with a CDR score of 1. All healthy controls were cognitively normal, free of neurological disease, and had no cognitive complaints. Every participant received a standard set of neuropsychological assessments including Mini-Mental Screening Examination (MMSE) (Folstein et al., 1975), Chinese version verbal learning test (Lin et al., 2006), and modified Rey–Osterrieth Complex Figure Test (CFT) (Osterrieth, 1944). In detail, memory-related performance tests of verbal learning include the California Verbal Learning Test (CVLT) of Total Correct (CVLT-TC), Short Delay 30 s Free Recall (CVLT-SD), Long Delay 10 min Free Recall (CVLT-LD), and those of CFT include the CFT-Delayed Recall (CFT-Delay). The AD and NC groups had average MMSE scores of 20.92 (range, 14–27) and 28.83 (range, 27–30), respectively. The detailed clinical and demographic data for all subjects was shown in Table 1.

Image acquisition

MR data were acquired at 1.5T MR system (Excite II; GE Medical Systems) with an eight-channel head coil. To avoid motion artifact generated during the scan, the subject's head was immobilized with cushions inside the coil after the alignment. One hundred twenty-four contiguous axial T1-weighted (T1W) images (slice thickness = 1.5 mm) were acquired, which was parallel to the anterior–posterior commissure (AC–PC) through the whole head by applying a three-dimensional fluid-attenuated inversion-recovery fast spoiled-gradient recalled echo (FLAIR-FSPGR) acquisition sequence (TR = 8.548 ms, TE = 1.836 ms, TI = 400 ms, flip angle = 15°, field of view = 26 cm × 26 cm, matrix size = 256 × 256) to aid the image registration. Fourteen diffusion tensor imaging volumes were obtained for each subject, including 13 volumes with diffusion gradients applied along 13 non-collinear directions ($b = 900$ s/mm^2) and one volume without diffusion weighting ($b = 0$). With the consideration of total brain coverage, each volume consisted of 70 contiguous axial slices (slice thickness = 2.2 mm) acquired, which was parallel to the AC–PC by using a single shot spin-echo echo planar imaging (EPI) sequence (TR = 17,000 ms, TE = 67 ms, number of excitation = 6, field of view = 26 cm × 26 cm, matrix size = 128 × 128). The total scanning time to collect the entire T1W and diffusion-weighted images was about 32 min for each subject.

Network construction

Nodes and edges are two basic elements of a network. To determine the nodes and edges of the brain networks, we undertook the following steps, which were similar to the procedure used in a previous study (Gong et al., 2009b).

Cortical parcellation. To determine the nodes of brain networks, we used the automated anatomical labeling (AAL) template (Tzourio-Mazoyer et al., 2002) to parcellate the whole cerebral cortex into 78 areas (39 regions in each hemisphere) (supplemental Table 1, available at www.jneurosci.org as supplemental material). Briefly, a specific customized group T1 template was first created to reduce the error term resulting from image registration and bias in template selection. This involved spatially normalizing each structural MR image to the ICBM 152 template in Montreal Neurological Institute (MNI) space. The optimum 12-parameter affine transformation was used in this step. All the normalized T1W images were then averaged and smoothed with an isotropic 8 mm full-width at half-maximum (FWHM) Gaussian kernel, and the customized template was created. Second, the T1W images of individual subjects were coregistered to their non-diffusion-weighted ($b = 0$) images based on normalized mutual information as the cost function. The coregistered T1W images were transformed to the same stereotactic space as the customized template image by applying an affine transformation with 12 degrees of freedom together with a series of nonlinear warps characterized by a set of 7 × 8 × 7 basis functions. The derived transformation parameters were then inverted and used to warp the AAL labels from MNI space to diffusion image native space with nearest-neighbor interpolation (Fig. 1). All the image processes, including image registration, spatial normalization, and customized template creation, were manipulated using Statistical Parametric Mapping 2 (SPM2) (Wellcome Department of Cognitive Neurology) in MATLAB6.5 (MathWorks).

Diffusion MRI tractography. To determine the edges of brain networks, we used diffusion MRI tractography methods. Briefly, the diffusion-weighted images were first registered to the non-diffusion-weighted (reference) images by using affine transformations to minimize distortions due to the eddy currents (Smith, 2002). Then, the diffusion tensor model was calculated by using an in-house program to get three eigenvectors and three eigenvalues. The whole-brain fiber tracking was performed via Fiber Assignment by Continuous Tracking (FACT) algorithm (Mori et al., 1999) from the center of each voxel as the seed point, with the fractional anisotropy (FA) threshold of 0.2 and tracking turning angular threshold of 60° between two connections. The corticocortical connections were established if any fiber bundle pass through or end in the corresponding cortical regions. With this tracking algorithm, there is the possibility of returning pseudoconnections because FACT streamline algorithm is sensitive to image resolution and noise. The possible
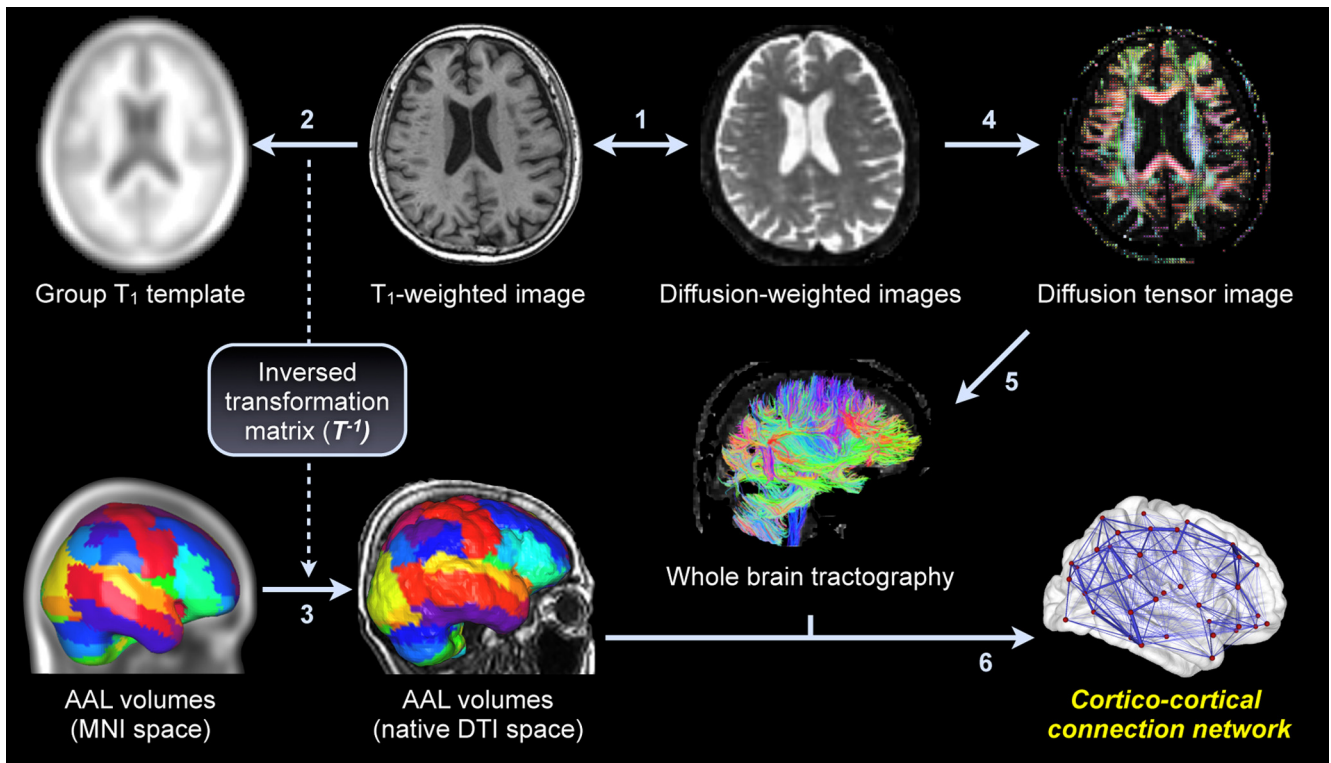
Figure 1. A flowchart of WM network construction. (1) Individual T1-weighted image were registered to the corresponding non-diffusion-weighted ($b = 0$) images using a 12 degrees of freedom affine transformation. (2) To obtain the transformation matrix (**T**), the coregistered T1-weighted images were registered to the customized group T1 template, which was in MNI space, by applying a nonlinear spatial normalization. (3) The inverse transformation matrix ($\mathbf{T}^{-1}$) was applied to the AAL atlas to generate corresponding AAL volumes in each individual's diffusion-weighted image native space. (4) The construction of DTI from diffusion-weighted images. The color-coded map represents the directions of first eigenvectors: red, left–right; green, anterior–posterior; blue, inferior–superior. (5) Fiber pathways were performed using fiber assignment by continuous tracking (FACT) algorithm to reconstruct whole-brain tractography. (6) Network constructions by determining the white matter connections for each pair of AAL volumes.

pseudoconnections may occur if there are only a few fiber bundles connected to a pair of cortical regions. To reduce influence from pseudoconnections, a threshold of three fibers was set to ensure the major connections among cortical regions (Li et al., 2009; Shu et al., 2009), i.e., the edge would be built up between a pair of nodes if at least three fibers were connected. In this study, the weighted WM networks were constructed with considering the fiber number (FN) and FA as the weight of each edge. The number of connections performed with streamline tracking may reflect the WM structure (Houenou et al., 2007), and has been used as a weight of network edges (Hagmann et al., 2007; Li et al., 2009). On the other hand, the FA value is an important index to evaluate fiber integrity (Basser and Pierpaoli, 1996; Beaulieu, 2002) and has a high correlation with conductivity (Tuch et al., 2001). To reveal the situations of WM structure, the value of multiplying FN by the mean FA along the fiber bundles connected a pair of cortical regions (node i and node j) was used to weight the edge, w_{ij}. In this way, if there are two pairs of cortical regions connecting with the same fiber number, the weights of the edges would be different while the FA values are considered here.

Network analysis
Small-world properties. Small-world network parameters (clustering coefficient, C_p, and shortest path length, L_p) were originally proposed by Watts and Strogatz (1998). In this study, we investigated the small-world properties of the weighted brain networks. The weighted clustering coefficient of a node i, $C^w(i)$, which was defined as the likelihood whether the neighborhoods were connected with each other or not (Onnela et al., 2005), is expressed as follows:

$$C^w(i) = \frac{2}{k_i(k_i - 1)} \sum_{j,k} (\bar{w}_{ij}\bar{w}_{jk}\bar{w}_{ki})^{1/3},$$

where k_i is the degree of node i, and $\bar{w}$ is the weight, which is scaled by the mean of all weights to control each participant's cost at the same level. The clustering coefficient is zero, $C^w(i) = 0$, if the nodes are isolated or with just one connection, i.e., $k_i = 0$ or $k_i = 1$. The weighted clustering coefficient, C_p^w, of a network is the average of the clustering coefficient over all nodes, which indicates the extent of local interconnectivity or cliquishness in a network (Watts and Strogatz, 1998). The path length between any pair of nodes (e.g., node i and node j) is defined as the sum of the edge lengths along this path. For weighted networks, the length of each weighted edge was assigned by computing the reciprocal of the edge weight, $1/\bar{w}$. The weighted shortest path length, $L^w(i,j)$, is defined as the length of the path for node i and node j with the shortest length. We used the weighted characteristic shortest path length, L^w, of a network by using a "harmonic mean" length between pairs (Newman, 2003), that is, the reciprocal of the average of the reciprocals for all nodes in the network. The weighted characteristic shortest path length of a network is computed as follows:

$$L_p^w = \frac{1}{N(N-1)} \sum_{i=1}^{N} \sum_{j \neq i}^{N} \frac{1}{L^w(i, j)},$$

where N is the number of nodes in the network. The L_p^w of a network quantifies the ability for information propagation in parallel. To examine the small-world properties, the weighted clustering coefficient, C_p^w, and weighted characteristic shortest path length, L_p^w, of the brain networks were compared with those of random networks. In this study, we generated 100 matched random networks, which had the same number of nodes, edges, and degree distribution as the real networks (Maslov and Sneppen, 2002). Of note, we retained the weight of each edge during the randomization procedure such that the weight distribution of the net-
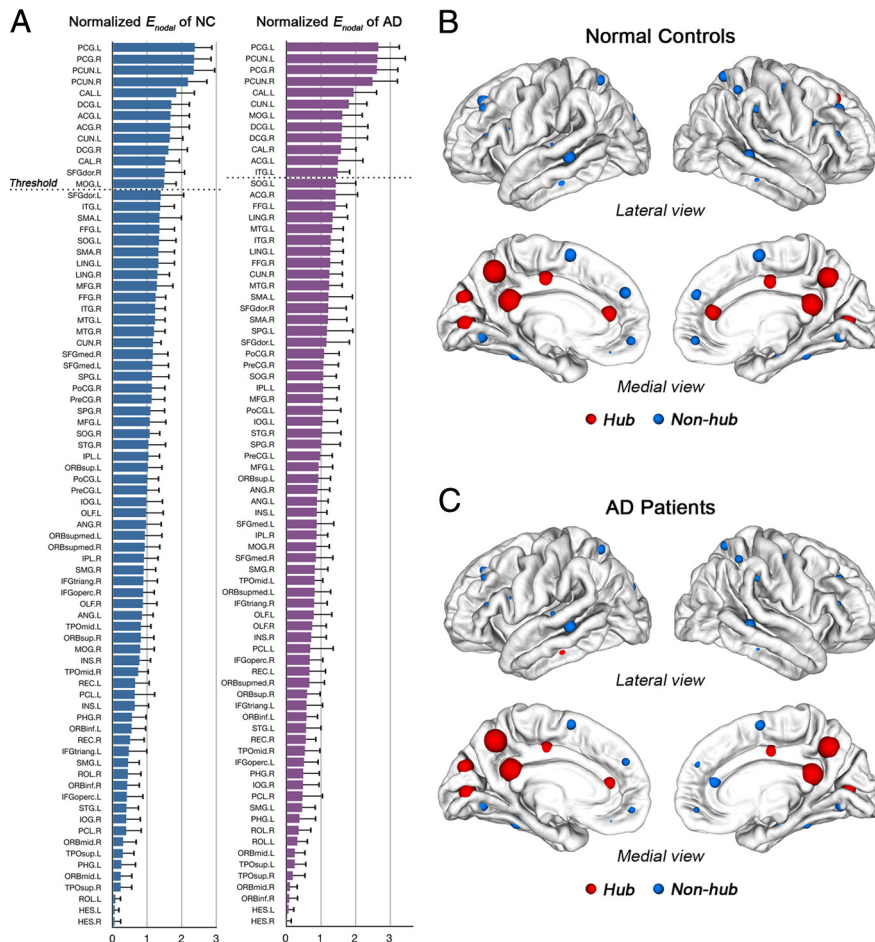
Figure 2. The global network hubs with high nodal efficiency in AD patients and NCs. A hub region, for node i, was identified if the mean of $E_{nodal}(i)$ was larger than the sum of the mean and SD of all $E_{nodal}(i)$. ***A***, The normalized nodal efficiency (divided by mean of all nodes, $\bar{E}_{nodal}$) for all 78 cortical regions sorted by the mean in a descending order; the dashed line indicates the threshold (mean + SD) for hub identification. Hub and nonhub regions of NC networks (***B***) and AD networks (***C***) with node sizes indicating their node efficiency values are mapped onto the cortical surfaces at the lateral and medial views, respectively, by using the Visualization Toolkit (VTK, www.vtk.org) library. Notably, the regions are located according to their centroid stereotaxic coordinates. For the abbreviations, see supplemental Table 1 (available at www.jneurosci.org as supplemental material).

where $E_{glob}(G_i)$ is the global efficiency of the neighborhood subgraph G_i of the node i, is expressed as follows:

$$E_{glob}(G_i) = \frac{1}{N_{G_i}(N_{G_i} - 1)} \sum_{j,k \in G_i} \frac{1}{L^W(j, k)}.$$

The local efficiency reflects how much the network is fault tolerant and how well the information is transferred within the neighbors of a given node. In brain network analysis, the efficiency measurement has many conceptual and technical advantages over the conventional small-world metrics (i.e., C_p^w and L_p^w), since it provides a single measure to deal with the local and global organization of the network (Latora and Marchiori, 2003; Achard and Bullmore, 2007; He et al., 2009).

Nodal characteristics. To determine the nodal (regional) characteristics of structural cortical networks, we computed the nodal efficiency (E_{nodal}) for examining the regional connections. The nodal efficiency for a given node i ($E_{nodal}(i)$) was defined as the inverse of the harmonic mean of the shortest path length between this node and all other nodes in the network (Achard and Bullmore, 2007), which is as follows:

$$E_{nodal}(i) = \frac{1}{N-1} \sum_{i \neq j \in G} \frac{1}{L^w(i, j)},$$

where the $L^w(i,j)$ is the weighted shortest path length between node i and node j in G. E_{nodal} quantifies the importance of the nodes for the communication within the network. Moreover, the nodes with high E_{nodal} values can be categorized as hubs in a network (Achard and Bullmore, 2007).

Statistical analysis

To determine the between-group differences in the small-world properties (the weighted clustering coefficient, C_p^w, the weighted characteristic shortest path length, L_p^w, the normalized weighted clustering coefficient, γ, and the normalized weighted characteristic shortest path length, λ) and network efficiency (the local efficiency, E_{loc}, and the global efficiency, E_{glob}), a linear regression analysis was separately performed on each network metric. Age and sex were taken as covariates in this model. Likewise, such an analysis was also applied to nodal efficiency, E_{nodal}, of all 78 cortical regions. A false discovery rate (FDR) procedure was further performed at a q value of 0.05 to correct for multiple comparisons (Genovese et al., 2002). Finally, we examined the relationship between the network metrics and the cognitive and memory performances in both groups separately with controlling the age and sex as the confounding variables. Here, the tests of the cognitive and memory performances include MMSE, CVLT-TC, CVLT-SD, CVLT-LD, and CFT-Delay.

work was preserved. Furthermore, we computed the normalized weighted clustering coefficient, $\gamma = C_p^w/C_p^{w\text{-rand}}$, and the normalized weighted characteristic shortest path length, $\lambda = L_p^w/L_p^{w\text{-rand}}$, where $C_p^{w\text{-rand}}$ and $L_p^{w\text{-rand}}$ are the mean weighted clustering coefficient and the mean weighted characteristic shortest path length of 100 matched random networks. Of note, the two parameters (i.e., γ and λ) correct the differences in the edge number and degree distribution of the networks across individuals. A real network would be considered small-world if $\gamma \gg 1$ and $\lambda \approx 1$ (Watts and Strogatz, 1998). In other words, a small-world network has not only the higher local interconnectivity but also the approximately equivalent characteristic shortest path length compared with the random networks. These two measurements can be summarized into a simple quantitative metric, small-worldness, $\sigma = \gamma/\lambda > 1$ (Humphries et al., 2006).

Network efficiency. The global efficiency of a network, E_{glob}, is defined by the inverse of the harmonic mean of the shortest path length between each pair of nodes within the network (Latora and Marchiori, 2003), i.e., $E_{glob} = 1/L_p^w$. The local efficiency of a network, E_{loc}, is defined as the average of the local efficiencies of each node (Latora and Marchiori, 2003), that is,

$$E_{loc}(G) = \frac{1}{N} \sum_{i \in G} E_{glob}(G_i),$$

Results
Demographics
There were no significant differences in age ($p = 0.169$) and gender ($p = 0.8$) between AD patients and controls. For the neuropsychological tests, there were significant between-group differences in MMSE scores ($p < 1.0 \times 10^{-22}$), CVLT-TC ($p < 1.0 \times 10^{-18}$), CVLT-SD ($p < 1.0 \times 10^{-19}$), CVLT-LD ($p < 1.0 \times 10^{-28}$), and CFT-Delay ($p < 1.0 \times 10^{-17}$) (Table 1).

Small-world properties of human WM networks
Small-world model
In a small-world network, the nodes usually have a great local interconnectivity compared with a random network ($\gamma \gg 1$), and the shortest path length between any pair of nodes is approximately equivalent to a comparable random network ($\lambda \approx 1$) (Watts and Strogatz, 1998). To clarify the small-world characteristics of WM network, we calculated the weighted clustering coefficient, C_p^w, and the weighted characteristic shortest path length, L_p^w, of the brain network and compared it with those of the corresponding random networks. Our results showed that the weighted clustering coefficients of brain structural network were about four times larger than the random network ($\gamma_{AD} = 4.18 \pm 0.56$, $\gamma_{NC} = 4.03 \pm 0.43$), and the weighted characteristic shortest path lengths were approximately equivalent to the random network ($\lambda_{AD} = 1.48 \pm 0.10$, $\lambda_{NC} = 1.42 \pm 0.09$) for each group. The small-worldness ($\sigma = \gamma/\lambda$) calculated from these indices was also larger than 1 ($\sigma_{AD} = 2.83 \pm 0.33$, $\sigma_{NC} = 2.85 \pm 0.34$). These results suggest that both AD patients and controls had prominent small-world properties in WM networks, which were consistent with previous diffusion-MRI studies in healthy subjects (Hagmann et al., 2007; Gong et al., 2009a,b; Li et al., 2009; Shu et al., 2009).

AD-related alterations
Using linear regression analysis with the age and sex as the covariates, we found that the weighted clustering coefficient, C_p^w, the normalized weighted clustering coefficient, γ, and the small-worldness, σ, had no significant differences between the AD and NC groups (all $p > 0.25$). However, we observed that AD networks had increased weighted characteristic shortest path length, L_p^w ($t_{(51)} = 2.685$, $p = 0.010$, Cohen's $d = 0.724$), and the normalized weighted characteristic shortest path length, λ ($t_{(51)} = 2.302$, $p = 0.025$, Cohen's $d = 0.610$), in WM networks as compared to the controls. For efficiency measurements, the local efficiency and global efficiency of brain networks were computed. Compared with the controls, WM networks of AD patients showed no significant changes in the local efficiency, E_{loc} ($t_{(51)} = -1.515$, $p = 0.136$), but showed significantly reduced global efficiency, E_{glob} ($t_{(51)} = -2.770$, $p = 0.008$, Cohen's $d = 0.759$). These results imply that the small-world architecture and network efficiency were significantly altered in WM networks of AD patients.

Regional nodal characteristics
Hub regions
In this study, the nodal efficiency, E_{nodal}, was computed to examine the nodal characteristics of each cortical region in WM anatomical network. Figure 2 shows the normalized nodal efficiency (divided by the mean of all nodes, $\bar{E}_{nodal}$) for all 78 cortical regions sorted by the mean in a descending order (Fig. 2A), and the nodes with size of $\bar{E}_{nodal}$ on the cortical surfaces (Fig. 2B,C). The regions with high E_{nodal} imply pivotal roles for the communication between any pair of nodes of the brain network (Albert and Barabasi, 2002; Achard and Bullmore, 2007; Gong et al., 2009b). Specifically, in the present study, the regions were defined as network hubs if their nodal efficiency, E_{nodal}, was 1 SD greater
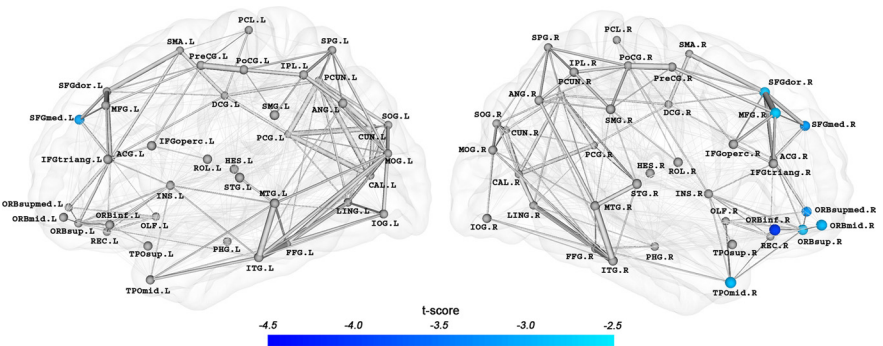
Figure 3. Regions with significant differences in nodal efficiency between AD patients and NCs. The brain regions showing significant group difference in nodal efficiency are mapped onto the cortical surfaces at the lateral view, by using the Visualization Toolkit (VTK, www.vtk.org) library. Notably, the network shown here was constructed by averaging the anatomical connection matrices of all subjects. The nodal regions are located according to their centroid stereotaxic coordinates. The edge widths represent the strengths of the connections between nodes. The statistical criterion for between-group differences was set at $p < 0.05$ (FDR-corrected). The color bar represents t values of group comparison after removing the effects of age and sex. For the abbreviations of nodes, see supplemental Table 1 (available at www.jneurosci.org as supplemental material).

Table 2. Regions with AD-related changes in nodal efficiency

Region	Category	t statistic
Right inferior frontal gyrus, orbital part	Paralimbic	−4.05
Right superior frontal gyrus, medial orbital	Paralimbic	−3.30
Right superior frontal gyrus, medial	Association	−3.26
Left superior frontal gyrus, medial	Association	−3.18
Right middle frontal gyrus, orbital part	Paralimbic	−3.06
Right temporal pole: middle temporal gyrus	Paralimbic	−3.03
Right superior frontal gyrus, orbital part	Paralimbic	−3.01
Right superior frontal gyrus, dorsolateral	Association	−2.98
Right middle frontal gyrus	Association	−2.93

The regions with significant decreased nodal efficiency ($p < 0.05$, FDR-corrected) are listed in ascending order by t scores. The cortical regions were classified as primary, association, and paralimbic (Mesulam, 1998).

than the average of the network [i.e., $\bar{E}_{nodal}(i) > (\text{mean} + \text{SD})$] (Fig. 2A, dashed line)].

In the NC group, 13 hub regions were identified, including 5 association cortex regions, 6 paralimbic cortex regions, and 2 primary cortex regions (Fig. 2A,B; supplemental Table 2, available at www.jneurosci.org as supplemental material). In the AD group, 12 hub regions were identified, including 5 association cortex regions, 5 paralimbic cortex regions, and 2 primary cortex regions (Fig. 2A,C; supplemental Table 3, available at www.jneurosci.org as supplemental material). In both groups, 11 brain regions (bilateral PCG, PCUN, median cingulate and paracingulate gyri, calcarine fissure and surrounding cortex, left cuneus, anterior cingulate and paracingulate gyri, and middle occipital gyrus) were identified as hubs in common (Fig. 2). It was worthy to note that both PCUN and PCG were identified as the most important regions in WM networks of AD and controls, which was consistent with the previous diffusion-MRI tractography network analysis in healthy adults (Hagmann et al., 2007; Gong et al., 2009a,b; Shu et al., 2009).

AD-related alterations
We further compared the nodal efficiency of cortical regions in WM networks between the two groups. We found that AD networks showed decreased nodal efficiency ($p < 0.05$, FDR-corrected) predominantly located in the frontal regions, including four frontal association regions [bilateral medial part the superior frontal gyrus (SFGmed), right dorsolateral part of the superior frontal gyrus (SFGdor), and middle frontal gyrus (MFG)] and four frontal paralimbic regions [right orbital part of

Table 3. Partial correlation coefficient between small-world and efficiency metrics and cognitive performances

Network metric	Group	Partial correlation coefficient				
		MMSE	CVLT-TC	CVLT-SD	CVLT-LD	CFT-delay
C_p	AD	0.271	0.116	0.110	−0.032	0.057
	NC	0.172	−0.225	−0.211	−0.169	0.253
L_p	AD	−0.131	−0.519*	−0.552**	−0.169	−0.039
	NC	−0.105	0.004	0.017	0.040	−0.229
g	AD	0.147	−0.276	−0.493*	−0.271	0.031
	NC	−0.048	−0.103	−0.041	−0.075	−0.208
λ	AD	0.039	−0.470*	−0.392	0.134	0.015
	NC	0.105	0.296	0.295	0.282	−0.030
σ	AD	0.135	0.026	−0.242	−0.363	0.016
	NC	−0.109	−0.257	−0.188	−0.220	−0.179
E_{loc}	AD	−0.197	0.307	0.464*	0.068	0.034
	NC	0.075	−0.111	−0.081	−0.031	0.274
E_{glob}	AD	0.075	0.537**	0.561**	0.178	−0.024
	NC	0.140	−0.023	−0.032	−0.022	0.221

The partial correlations were computed with age and sex as the confounding covariates. *$p < 0.05$, **$p < 0.01$.

Table 4. Partial correlation coefficient between regional nodal efficiency and cognitive performances

Network metric	Group	Partial correlation coefficient				
		MMSE	CVLT-TC	CVLT-SD	CVLT-LD	CFT-delay
E_{nodal} of SFGmed.L	AD	0.074	0.208	0.105	0.226	−0.007
	NC	0.100	0.094	0.086	0.224	0.265
E_{nodal} of SFGdor.R	AD	0.103	0.505*	0.318	0.111	−0.128
	NC	0.114	0.125	0.184	0.157	0.108
E_{nodal} of ORBsup.R	AD	0.092	0.078	0.144	0.229	−0.035
	NC	0.202	0.058	−0.087	−0.087	0.149
E_{nodal} of MFG.R	AD	0.087	0.522*	0.360	−0.003	−0.023
	NC	0.036	0.055	0.175	0.104	0.103
E_{nodal} of ORBmid.R	AD	0.439*	−0.015	0.177	0.152	0.161
	NC	0.134	−0.101	−0.154	−0.108	−0.060
E_{nodal} of ORBinf.R	AD	0.329	0.118	0.094	0.289	−0.094
	NC	0.299	−0.072	−0.159	−0.143	−0.168
E_{nodal} of SFGmed.R	AD	0.219	0.354	0.183	0.175	−0.094
	NC	0.241	0.110	0.166	0.174	0.129
E_{nodal} of ORBsupmed.R	AD	0.037	0.238	0.171	0.054	−0.105
	NC	0.161	0.050	0.083	0.160	0.155
E_{nodal} of TPOmid.R	AD	−0.138	0.450*	0.441*	−0.018	−0.035
	NC	0.289	0.227	0.020	0.232	0.308

The partial correlations were computed with age and sex as the confounding covariates. *$p < 0.05$. For the abbreviations, see supplemental Table 1 (available at www.jneurosci.org as supplemental material).

the inferior frontal gyrus (ORBinf), orbital, medial orbital part of the superior frontal gyrus (ORBsup, ORBsupmed), and orbital part of the middle frontal gyrus (ORBmid)]. Additionally, we also found decreased nodal efficiency in one temporal lobe region [the temporal pole of the middle temporal gyrus (TPOmid)] (Fig. 3, Table 2). The findings indicated that the reduced nodal efficiency in AD patients was mainly located in the frontal cortical regions, which was compatible with the previous DTI studies showing abnormal WM integrity in these areas (Bozzali et al., 2002; Choi et al., 2005; Naggara et al., 2006; Xie et al., 2006).

Network properties correlation with cognition
We next examined the relationships of the network metrics (small-world and efficiency metrics) and the cognitive and memory performances. For nodal characteristics, we examined only the nodes with significant between-group differences (i.e., cortical regions listed in Table 2). To determine the relationships, partial correlation analysis with age and sex as confounding covariates were separately performed for the AD and NC groups. The results of the correlational analysis for network metrics are listed in Table 3 for global properties and in Table 4 for nodal characteristics. In the NC group, all of the cognitive and memory performances showed no significant correlation with the net-

work metrics. The following descriptions focus on the results in the AD group. Figure 4 shows the significant correlations between small-world and efficiency metrics and cognitive performances, and Figure 5 shows the significant correlations between regional nodal efficiency and cognitive performances in AD patients.

MMSE
There were no significant correlations between the small-world and network efficiency parameters and MMSE scores. In nodal characteristics, we observed that there was a significant positive correlation between MMSE scores and nodal efficiency ($r = 0.439$, $p = 0.036$) of the right ORBmid.

CVLT
The verbal memory tests, including CVLT-TC, CVLT-SD, and CVLT-LD, were selected as the memory performance of participants. First, we found that CVLT-TC was significantly negatively correlated with weighted shortest path length ($r = −0.509$, $p = 0.011$) and normalized weighted shortest path length ($r = −0.470$, $p = 0.024$), and significantly positively correlated with the global efficiency ($r = 0.537$, $p = 0.008$). This score was also significantly positively correlated with the nodal efficiency of the
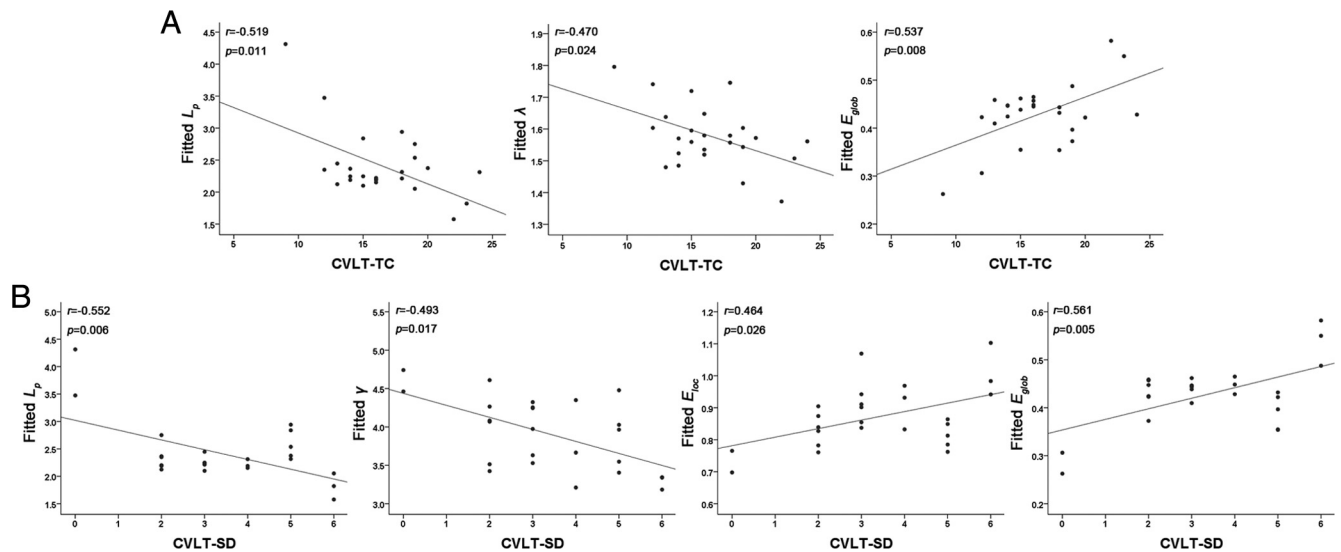
Figure 4. Scatter plots of small-world and efficiency metrics and memory performances in AD patients. ***A***, The significant correlations between CVLT-TC and L_p, λ, and E_{glob}. ***B***, The significant correlations between CVLT-SD and L_p, γ, E_{loc}, and E_{glob}.

right SFGdor ($r = 0.505$, $p = 0.014$), MFG ($r = 0.522$, $p = 0.011$), and TPOmid ($r = 0.45$, $p = 0.031$). Second, CVLT-SD was significantly negatively correlated with the weighted shortest path length ($r = -0.552$, $p = 0.006$) and normalized weighted clustering coefficient ($r = -0.493$, $p = 0.017$), and significantly positively correlated with the local efficiency ($r = 0.464$, $p = 0.026$) and the global efficiency ($r = 0.561$, $p = 0.005$). Also, we found that CVLT-SD was significantly negatively correlated with the nodal efficiency of right TPOmid ($r = 0.441$, $p = 0.035$). Finally, there were no significant correlations between CVLT-LD and any network metrics.
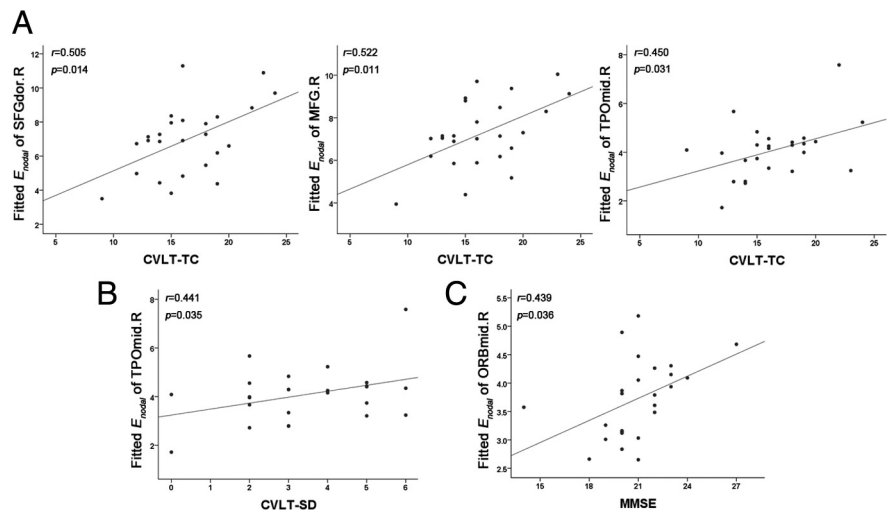
CFT-Delay
For this visual memory performance, we did not find any significant correlations between CFT-Delay and any network metrics.

Figure 5. Scatter plots of regional nodal efficiency and memory performances in AD patients. ***A***, The significant correlations between CVLT-TC and nodal efficiency of right SFGdor, MFG, and TPOmid. ***B***, The significant correlation between CVLT-SD and right TPOmid. ***C***, The significant correlation between MMSE and right ORBmid. For the abbreviations of nodes, see supplemental Table 1 (available at www.jneurosci.org as supplemental material).

Discussion
The present study used diffusion MRI tractography to demonstrate alterations in the topological organization of WM networks in AD patients. Our main findings are as follows: (1) the global topological organization of WM corticocortical connection network in AD patients was significantly disrupted as indicated by abnormal small-world properties and topological efficiency; (2) the regional characteristics (nodal efficiency) were altered in AD patients predominantly in the frontal cortical regions; and (3) changes in various network properties in AD patients were associated with the performance of behavior functions. These findings support the hypothesis that WM degeneration changes the structural connectivity pattern of WM network in AD.

Small-world structure in anatomical brain networks in AD
Our results showed that structural brain networks of both AD patients and NCs have a small-world topology, which is consis-

tent with the previous WM network studies by diffusion MRI (Hagmann et al., 2007, 2008; Gong et al., 2009a,b; Li et al., 2009; Shu et al., 2009). We found that, although WM networks of AD patients showed prominent small-world attributes, several network parameters (L_p^w, λ, and E_{glob}) were found to be significantly altered. The increased L_p^w and λ were consistent with the AD-related brain network studies using structural MRI (sMRI) (He et al., 2008), EEG (Stam et al., 2007), and MEG (Stam et al., 2009) (Table 5). Short path length ensures inter-regional effective integrity or prompt transfers of information in brain networks that is believed to constitute the basis of cognitive processes (Sporns and Zwi, 2004). Compared with the small-world properties of matched random networks, λ also showed an increased ratio of characteristic shortest path length predominantly in the AD group. The AD-related increases in the shortest path length could be attributable to the degeneration of fiber bundles for information transmission. These phenomena suggest that the connec-

Table 5. AD-related alterations of topological properties in the brain networks in the current study and previous studies

Study	Modality	Connectivity methods	Network type	Matrix size	Main findings					
					C_p	L_p	γ	λ	E_{loc}	E_{glob}
Current study	DTI	Tractography	Weighted	78	NS	▲	NS	▲	NS	▼
He et al. (2008)	sMRI	Partial correlation	Binary	54	▲	▲	—	—	—	—
Stam et al. (2007)	EEG	Synchronization likelihood	Binary	21	NS	▲	NS	▲	—	—
de Haan et al. (2009)	EEG	Synchronization likelihood	Weighted	21	—	—	▼	▼	—	—
Stam et al. (2009)	MEG	Phase lag index	Weighted	149	▼	▲	▼	▼	—	—
Supekar et al. (2008)	fMRI	Wavelet correlation	Binary	90	—	—	▼	NS	—	—

NS, Nonsignificant; ▲, AD > NC; ▼, AD < NC.

tions between cortical areas have been changed with less strength (reduced WM integrity) or longer pathway (disconnection). Given that the small-world topology is an optimal balance between local specialization and global integration when networks evolved for high complexity of dynamic behavior (Sporns et al., 2000), our findings of increased path length in AD networks indicate an imbalanced structure with reduced global efficiency for signal propagation among distant regions with more regular configuration in WM networks.

Previous studies of graph theoretical analysis using different modalities have demonstrated alterations of small-world topological parameters in AD (Table 5). Overall, the most consistent alteration in these studies was the increased characteristic path length in AD-related networks. For example, the structural network study using sMRI reported by He et al. (2008) showed that the clustering coefficient and characteristic shortest path length were significantly increased in the AD patients as compared to the controls. In an EEG study, Stam et al. (2007) observed that the brain functional networks of AD patients had increased both characteristic shortest path length and normalized characteristic shortest path length. These results are consistent with our findings. In contrast, it has been found to exhibit decreased normalized clustering coefficient and/or normalized characteristic path length in brain functional networks of AD patients with fMRI (Supekar et al., 2008), EEG (de Haan et al., 2009), and MEG (Stam et al., 2009). Notably, there were still some conflicts with the same modality like EEG (Stam et al., 2007; de Haan et al., 2009). These discrepancies in brain network analysis could be due to the different populations, network construction methods (e.g., EEG, MEG, fMRI, sMRI, and DTI) and network analytic tools (unweighted or weighted). Here, we emphasized that the present study for the first time used the diffusion MRI tractography to show small-world alteration in WM network in AD.

Regional characteristics in anatomical brain networks in AD
The regional alterations in AD networks were also found to have significantly decreased nodal characteristics (i.e., E_{nodal}) in cortical regions (Table 2), which were predominately located in the frontal lobe (e.g., ORBinf, SFGmed, and MFG) and temporal lobe (e.g., TPOmid). The frontal regions are thought to be involved in the emotional, memory, and executive functions (Stuss and Alexander, 2000; Baddeley, 2003). Many previous studies have demonstrated that these frontal regions exhibited AD-related abnormalities in the WM integrity (Bozzali et al., 2002; Choi et al., 2005), gray matter morphology (Honea et al., 2010), and functional interactions (Horwitz et al., 1987; Grady et al., 2001, 2003; Wang et al., 2007). The temporal pole, which involves linguistic integration, emotion, and semantic memory (Dupont, 2002; Olson et al., 2007), has been also indicated in that there was the atrophy and neuronal loss (Arnold et al., 1994; Galton et al., 2001) in AD patients. Using graph theoretical analysis, our results

show that the frontal and temporal cortices have decreased nodal efficiency in WM networks, which reflected the WM abnormality of the connections in these cortical regions. Notably, decreased efficiency in the frontal regions was mainly located in the right hemisphere. Previous studies have shown that the decreased activity of right prefrontal regions are associated with the worse memory performance in AD patients (Grady et al., 2001; Lekeu et al., 2003), implying that the structural decline in the right hemisphere likely links with the memory loss. Together, our results suggest that the WM degenerated alterations in these frontal regions might influence information transmission and functional integration for AD patients.

Relationship between network properties and the cognitive and memory performances
By examining the correlation between network metrics and cognitive performances, our results indicated that the AD-related alterations of network properties were associated with the decline of cognitive functions. We found that AD patients with longer shortest path length and decreased global efficiency in WM network had lower verbal memory performance (e.g., CVLT-TC and CVLT-SD). Also, AD patients with reduced regional efficiency of several cortical regions (e.g., SFGdor, MFG, and ORBmid) in WM network had lower cognitive/memory functions (e.g., MMSE scores, CVLT-TC, and CVLT-SD). High correlations between network properties and the behavioral scores indicate that the network properties are highly associated with the disrupted cognitive/memory functions. Previous studies have demonstrated that human structural connectivity is closely related to functional connectivity (Hagmann et al., 2008) (for review, see Damoiseaux and Greicius, 2009) and underlies high-order cognitive activities (for review, see Minati et al., 2007) (Li et al., 2009). Thus our results of disrupted WM connectivity likely reflect the breakdown of function connections that influences cognitive performances of the patients.

Methodological issues
There are some methodological issues to be considered. First, the connection between each pair of cortical areas was set at a threshold of three fibers to construct the brain networks. To test the influences by threshold selection, we examined the results by choosing a range from one to five for threshold, and the results were very stable in this range. Second, we constructed brain weighted anatomical networks with assigning a weight index (FN × FA) to each edge. In this study, we also constructed the FN weighted network and FA weighted network to explore the differences between two groups, and the results were similar to our main findings (supplemental Tables 4, 5 and supplemental Text 1, available at www.jneurosci.org as supplemental material). Third, we used the AAL atlas to parcellate the brain cortical regions for large-scale network construction. Recent studies have

suggested that the node definition by different parcellation schemes would produce different properties of brain networks (Hagmann et al., 2008; Wang et al., 2009; Hayasaka and Laurienti, 2010; Zalesky et al., 2010); these might provide different information for the alterations of AD networks. Fourth, streamline tractography was used to construct WM networks in the present study. Subcortical regions such as the hippocampus and the thalamus were not studied, because the complex tissue structure with the uncertainty of the principal eigenvector would increase the errors of streamline tractography. Recently, probabilistic tractography has been used to identify the connections for subcortical and cortical regions (Behrens et al., 2003), and to construct the human brain anatomical networks (Iturria-Medina et al., 2008; Gong et al., 2009a). These might provide distinct information for anatomical connectivity patterns of brain networks. Fifth, we examined changes in the anatomical networks in AD. It has been suggested that anatomical networks of the human brain share similar topological features (e.g., network hubs) with functional networks constructed from fMRI (Damoiseaux and Greicius, 2009; Honey et al., 2009), implying a close association between brain structure and function. The integration of different modalities (e.g., DTI and fMRI) could allow us to look into how the alterations of anatomical networks are associated with changes in functional networks. Sixth, the topological changes of WM network were demonstrated in AD, but the relationship between network properties and disease progression or other dementia types is currently unclear. Further studies on mild cognitive impairment (the transit state between healthy elderly and AD) and other dementia types such as frontotemporal dementia and dementia with Lewy bodies will be helpful to clarify this issue. Finally, we used a cross-sectional design to show AD-related alterations in topological structure of WM networks. A longitudinal study would be vital to demonstrate progressive alterations of brain networks in AD.

Conclusion
In this study, we used diffusion MRI tractography to construct WM networks of AD patients and NCs, and demonstrated that the anatomical networks of both AD and NC groups exhibited small-world topology. More importantly, we showed that AD patients had significantly increased characteristic shortest path length and decreased global efficiency in WM networks, implying the WM dysconnectivity and topological disorganization in the AD networks. Specifically, we found that the AD patients had reduced nodal efficiency of cortical regions predominantly located in the frontal lobe. Finally, we showed that the alterations of AD patients were highly associated with the cognitive and memory performances. Our findings support the WM degeneration hypothesis of altered anatomical networks in AD, and suggest that the alterations affect the cognitive functions of the patients. This topology-based analysis of the human brain WM networks provides a novel way to reveal the patterns of structural dysconnectivity in neurodegenerative diseases. The present study also has important implications for the understanding of human brain connectome in neuropsychiatric diseases (Sporns et al., 2005).

References
Achard S, Bullmore E (2007) Efficiency and cost of economical brain functional networks. PLoS Comput Biol 3:e17.

Albert R, Barabasi A (2002) Statistical mechanics of complex networks. Rev Mod Phys 74:47–97.

Arnold SE, Hyman BT, Van Hoesen GW (1994) Neuropathologic changes of the temporal pole in Alzheimer's disease and Pick's disease. Arch Neurol 51:145–150.

Baddeley A (2003) Working memory: looking back and looking forward. Nat Rev Neurosci 4:829–839.

Basser PJ, Pierpaoli C (1996) Microstructural and physiological features of tissues elucidated by quantitative-diffusion-tensor MRI. J Magn Reson B 111:209–219.

Basser PJ, Mattiello J, LeBihan D (1994) MR diffusion tensor spectroscopy and imaging. Biophys J 66:259–267.

Beaulieu C (2002) The basis of anisotropic water diffusion in the nervous system—a technical review. NMR Biomed 15:435–455.

Behrens TE, Johansen-Berg H, Woolrich MW, Smith SM, Wheeler-Kingshott CA, Boulby PA, Barker GJ, Sillery EL, Sheehan K, Ciccarelli O, Thompson AJ, Brady JM, Matthews PM (2003) Non-invasive mapping of connections between human thalamus and cortex using diffusion imaging. Nat Neurosci 6:750–757.

Bozzali M, Falini A, Franceschi M, Cercignani M, Zuffi M, Scotti G, Comi G, Filippi M (2002) White matter damage in Alzheimer's disease assessed in vivo using diffusion tensor magnetic resonance imaging. J Neurol Neurosurg Psychiatry 72:742–746.

Brun A, Englund E (1986) Brain changes in dementia of Alzheimer's type relevant to new imaging diagnostic methods. Prog Neuropsychopharmacol Biol Psychiatry 10:297–308.

Bullmore E, Sporns O (2009) Complex brain networks: graph theoretical analysis of structural and functional systems. Nat Rev Neurosci 10:186–198.

Choi SJ, Lim KO, Monteiro I, Reisberg B (2005) Diffusion tensor imaging of frontal white matter microstructure in early Alzheimer's disease: a preliminary study. J Geriatr Psychiatry Neurol 18:12–19.

Damoiseaux JS, Greicius MD (2009) Greater than the sum of its parts: a review of studies combining structural connectivity and resting-state functional connectivity. Brain Struct Funct 213:525–533.

de Haan W, Pijnenburg YAL, Strijers RLM, van der Made Y, van der Flier WM, Scheltens P, Stam CJ (2009) Functional neural network analysis in frontotemporal dementia and Alzheimer's disease using EEG and graph theory. BMC Neurosci 10:101.

Delbeuck X, Van der Linden M, Collette F (2003) Alzheimer's disease as a disconnection syndrome? Neuropsychol Rev 13:79–92.

Dupont S (2002) Investigating temporal pole function by functional imaging. Epileptic Disord 4 [Suppl 1]:S17–S22.

Folstein MF, Folstein SE, McHugh PR (1975) "Mini-mental state." A practical method for grading the cognitive state of patients for the clinician. J Psychiatr Res 12:189–198.

Galton CJ, Gomez-Anson B, Antoun N, Scheltens P, Patterson K, Graves M, Sahakian BJ, Hodges JR (2001) Temporal lobe rating scale: application to Alzheimer's disease and frontotemporal dementia. J Neurol Neurosurg Psychiatry 70:165–173.

Genovese CR, Lazar NA, Nichols T (2002) Thresholding of statistical maps in functional neuroimaging using the false discovery rate. Neuroimage 15:870–878.

Gong G, Rosa-Neto P, Carbonell F, Chen ZJ, He Y, Evans AC (2009a) Age- and gender-related differences in the cortical anatomical network. J Neurosci 29:15684–15693.

Gong G, He Y, Concha L, Lebel C, Gross DW, Evans AC, Beaulieu C (2009b) Mapping anatomical connectivity patterns of human cerebral cortex using in vivo diffusion tensor imaging tractography. Cereb Cortex 19:524–536.

Grady CL, Furey ML, Pietrini P, Horwitz B, Rapoport SI (2001) Altered brain functional connectivity and impaired short-term memory in Alzheimer's disease. Brain 124:739–756.

Grady CL, McIntosh AR, Beig S, Keightley ML, Burian H, Black SE (2003) Evidence from functional neuroimaging of a compensatory prefrontal network in Alzheimer's disease. J Neurosci 23:986–993.

Hagmann P, Kurant M, Gigandet X, Thiran P, Wedeen VJ, Meuli R, Thiran JP (2007) Mapping human whole-brain structural networks with diffusion MRI. PLoS ONE 2:e597.

Hagmann P, Cammoun L, Gigandet X, Meuli R, Honey CJ, Wedeen VJ, Sporns O (2008) Mapping the structural core of human cerebral cortex. PLoS Biol 6:e159.

Hayasaka S, Laurienti PJ (2010) Comparison of characteristics between region- and voxel-based network analyses in resting-state fMRI data. Neuroimage 50:499–508.

He Y, Evans A (2010) Graph theoretical modeling of brain connectivity. Curr Opin Neurol 23:341–350.

He Y, Chen Z, Evans A (2008) Structural insights into aberrant topological patterns of large-scale cortical networks in Alzheimer's disease. J Neurosci 28:4756–4766.

He Y, Dagher A, Chen Z, Charil A, Zijdenbos A, Worsley K, Evans A (2009) Impaired small-world efficiency in structural cortical networks in multiple sclerosis associated with white matter lesion load. Brain 132:3366–3379.

Honea RA, Swerdlow RH, Vidoni ED, Goodwin J, Burns JM (2010) Reduced gray matter volume in normal adults with a maternal family history of Alzheimer disease. Neurology 74:113–120.

Honey CJ, Sporns O, Cammoun L, Gigandet X, Thiran JP, Meuli R, Hagmann P (2009) Predicting human resting-state functional connectivity from structural connectivity. Proc Natl Acad Sci U S A 106:2035–2040.

Horwitz B, Grady CL, Schlageter NL, Duara R, Rapoport SI (1987) Intercorrelations of regional cerebral glucose metabolic rates in Alzheimer's disease. Brain Res 407:294–306.

Houenou J, Wessa M, Douaud G, Leboyer M, Chanraud S, Perrin M, Poupon C, Martinot JL, Paillere-Martinot ML (2007) Increased white matter connectivity in euthymic bipolar patients: diffusion tensor tractography between the subgenual cingulate and the amygdalo-hippocampal complex. Mol Psychiatry 12:1001–1010.

Humphries MD, Gurney K, Prescott TJ (2006) The brainstem reticular formation is a small-world, not scale-free, network. Proc Biol Sci 273:503–511.

Iturria-Medina Y, Sotero RC, Canales-Rodríguez EJ, Alemán-Gómez Y, Melie-García L (2008) Studying the human brain anatomical network via diffusion-weighted MRI and graph theory. Neuroimage 40:1064–1076.

Kiuchi K, Morikawa M, Taoka T, Nagashima T, Yamauchi T, Makinodan M, Norimoto K, Hashimoto K, Kosaka J, Inoue Y, Inoue M, Kichikawa K, Kishimoto T (2009) Abnormalities of the uncinate fasciculus and posterior cingulate fasciculus in mild cognitive impairment and early Alzheimer's disease: a diffusion tensor tractography study. Brain Res 1287:184–191.

Latora V, Marchiori M (2003) Economic small-world behavior in weighted networks. Eur Phys J B Condens Matter Complex Syst 32:249–263.

Lekeu F, Van der Linden M, Chicherio C, Collette F, Degueldre C, Franck G, Moonen G, Salmon E (2003) Brain correlates of performance in a free/cued recall task with semantic encoding in Alzheimer disease. Alzheimer Dis Assoc Disord 17:35–45.

Li Y, Liu Y, Li J, Qin W, Li K, Yu C, Jiang T (2009) Brain anatomical network and intelligence. PLoS Comput Biol 5:e1000395.

Lin KN, Liu HC, Wang PN, Liao YC (2006) Early detection of memory impairment: the use of the 12-item selective reminding test in Taiwan. Paper presented at The 10th International Conference on Alzheimer's Disease and Related Disorders. Madrid, July.

Maslov S, Sneppen K (2002) Specificity and stability in topology of protein networks. Science 296:910–913.

McKhann G, Drachman D, Folstein M, Katzman R, Price D, Stadlan EM (1984) Clinical diagnosis of Alzheimer's disease: report of the NINCDS-ADRDA Work Group under the auspices of Department of Health and Human Services Task Force on Alzheimer's Disease. Neurology 34:939–944.

Mesulam MM (1998) From sensation to cognition. Brain 121:1013–1052.

Minati L, Grisoli M, Bruzzone MG (2007) MR spectroscopy, functional MRI, and diffusion-tensor imaging in the aging brain: a conceptual review. J Geriatr Psychiatry Neurol 20:3–21.

Mori S, van Zijl PC (2002) Fiber tracking: principles and strategies—a technical review. NMR Biomed 15:468–480.

Mori S, Crain BJ, Chacko VP, van Zijl PC (1999) Three-dimensional tracking of axonal projections in the brain by magnetic resonance imaging. Ann Neurol 45:265–269.

Morris JC (1993) The Clinical Dementia Rating (CDR): current version and scoring rules. Neurology 43:2412–2414.

Naggara O, Oppenheim C, Rieu D, Raoux N, Rodrigo S, Dalla Barba G, Meder JF (2006) Diffusion tensor imaging in early Alzheimer's disease. Psychiatry Res 146:243–249.

Newman MEJ (2003) The structure and function of complex networks. SIAM Rev 45:167–256.

Olson IR, Plotzker A, Ezzyat Y (2007) The enigmatic temporal pole: a review of findings on social and emotional processing. Brain 130:1718–1731.

Onnela JP, Saramäki J, Kertész J, Kaski K (2005) Intensity and coherence of motifs in weighted complex networks. Phys Rev E Stat Nonlin Soft Matter Phys 71:065103.

Osterrieth PA (1944) Le test de copie d'une figure complexe: contribution à l'étude de la perception et de la mémoire. Arch Psychol 30:286–356.

Pievani M, Agosta F, Pagani E, Canu E, Sala S, Absinta M, Geroldi C, Ganzola R, Frisoni GB, Filippi M (2010) Assessment of white matter tract damage in mild cognitive impairment and Alzheimer's disease. Hum Brain Mapp 31:1862–1875.

Rose SE, Chen F, Chalk JB, Zelaya FO, Strugnell WE, Benson M, Semple J, Doddrell DM (2000) Loss of connectivity in Alzheimer's disease: an evaluation of white matter tract integrity with colour coded MR diffusion tensor imaging. J Neurol Neurosurg Psychiatry 69:528–530.

Selkoe DJ (2002) Alzheimer's disease is a synaptic failure. Science 298:789–791.

Shu N, Liu Y, Li J, Li Y, Yu C, Jiang T (2009) Altered anatomical network in early blindness revealed by diffusion tensor tractography. PLoS ONE 4:e7228.

Smith SM (2002) Fast robust automated brain extraction. Hum Brain Mapp 17:143–155.

Sporns O, Zwi JD (2004) The small world of the cerebral cortex. Neuroinformatics 2:145–162.

Sporns O, Tononi G, Edelman GM (2000) Theoretical neuroanatomy: relating anatomical and functional connectivity in graphs and cortical connection matrices. Cereb Cortex 10:127–141.

Sporns O, Tononi G, Kötter R (2005) The human connectome: a structural description of the human brain. PLoS Comput Biol 1:e42.

Stam CJ, Jones BF, Nolte G, Breakspear M, Scheltens P (2007) Small-world networks and functional connectivity in Alzheimer's disease. Cereb Cortex 17:92–99.

Stam CJ, de Haan W, Daffertshofer A, Jones BF, Manshanden I, van Cappellen van Walsum AM, Montez T, Verbunt JPA, de Munck JC, van Dijk BW, Berendse HW, Scheltens P (2009) Graph theoretical analysis of magnetoencephalographic functional connectivity in Alzheimer's disease. Brain 132:213–224.

Stuss DT, Alexander MP (2000) Executive functions and the frontal lobes: a conceptual view. Psychol Res 63:289–298.

Supekar K, Menon V, Rubin D, Musen M, Greicius MD (2008) Network analysis of intrinsic functional brain connectivity in Alzheimer's disease. PLoS Comput Biol 4:e1000100.

Tuch DS, Wedeen VJ, Dale AM, George JS, Belliveau JW (2001) Conductivity tensor mapping of the human brain using diffusion tensor MRI. Proc Natl Acad Sci U S A 98:11697–11701.

Tzourio-Mazoyer N, Landeau B, Papathanassiou D, Crivello F, Etard O, Delcroix N, Mazoyer B, Joliot M (2002) Automated anatomical labeling of activations in SPM using a macroscopic anatomical parcellation of the MNI MRI single-subject brain. Neuroimage 15:273–289.

Ukmar M, Makuc E, Onor ML, Garbin G, Trevisiol M, Cova MA (2008) Evaluation of white matter damage in patients with Alzheimer's disease and in patients with mild cognitive impairment by using diffusion tensor imaging. Radiol Med 113:915–922.

Wang J, Wang L, Zang Y, Yang H, Tang H, Gong Q, Chen Z, Zhu C, He Y (2009) Parcellation-dependent small-world brain functional networks: a resting-state fMRI study. Hum Brain Mapp 30:1511–1523.

Wang K, Liang M, Wang L, Tian L, Zhang X, Li K, Jiang T (2007) Altered functional connectivity in early Alzheimer's disease: a resting-state fMRI study. Hum Brain Mapp 28:967–978.

Watts DJ, Strogatz SH (1998) Collective dynamics of 'small-world' networks. Nature 393:440–442.

Xie S, Xiao JX, Gong GL, Zang YF, Wang YH, Wu HK, Jiang XX (2006) Voxel-based detection of white matter abnormalities in mild Alzheimer disease. Neurology 66:1845–1849.

Yan C, Gong G, Wang J, Wang D, Liu D, Zhu C, Chen ZJ, Evans A, Zang Y, He Y (2010) Sex- and brain size-related small-world structural cortical networks in young adults: a DTI tractography study. Cereb Cortex. Advance online publication. Retrieved Aug. 5, 2010. doi:10.1093/cercor/bhq111.

Zalesky A, Fornito A, Harding IH, Cocchi L, Yücel M, Pantelis C, Bullmore ET (2010) Whole-brain anatomical networks: does the choice of nodes matter? Neuroimage 50:970–983.